Sulfide-associated hydrothermal dolomite and calcite reveal a shallow burial depth for Alpine-type Zn-(Pb) deposits

Sulfide-associated hydrothermal dolomite and calcite reveal a shallow burial depth for Alpine-type Zn-(Pb) deposits

M. Giorno[1], L. Barale[2], C. Bertok[1*], M. Frenzel[3], N. Looser[4], M. Guillong[4], S.M. Bernasconi[4] and L. Martire[1]

[1]Department of Earth Sciences, Università degli Studi di Torino, 10125 Turin, Italy

[2]IGG-CNR Torino, 10125 Turin, Italy

[3]Helmholtz-Zentrum Dresden-Rossendorf, Institute Freiberg for Resource Technology, 09599 Freiberg, Germany

[4]Department of Earth Sciences, ETH Zürich, 8092 Zürich, Switzerland

**E-mail: carlo.bertok@unito.it*

ABSTRACT

Difficulties in dating Mississippi Valley-type (MVT) mineral deposits and the often closely associated regional dolomitization events have led to considerable controversy regarding the tectonic settings in which they form. Here we report the first radiometric ages for an example of the Alpine subclass of MVT deposits: the Gorno district in Lombardy, Italy. U-Pb ages of hydrothermal carbonates pre- and post-dating the ore-forming event show that base-metal mineralization occurred shortly after the deposition of the Carnian host rocks. This implies that the Gorno ore deposits formed at shallow burial depth prior to the Early Jurassic western Tethys rifting phase. Contemporaneous Triassic magmatism and extensional tectonics likely contributed to the high geothermal heat fluxes required to drive the large-scale mineralizing system. The case of Gorno reinforces the necessity to base metallogenic models on reliable geochronological data

and warns against automatic extension of classic North American MVT models to similar deposits worldwide.

INTRODUCTION

Mississippi Valley-type (MVT) deposits are epigenetic, stratabound, carbonate-hosted sulfide bodies formed by high-salinity, warm fluids (75-200 °C, Leach et al., 2001; 2005). MVT mineral deposits and regional dolomitization events are often closely associated. Both are of major economic importance and are genetically related to hydrothermal fluid flow through large rock volumes. Since both the mineralization and the associated dolomitization events postdate host-rock deposition, stratigraphic constraints are generally not applicable to the determination of their ages, with few exceptions (e.g., mineralized clasts reworked in intraformational breccias; Schroll et al., 2006; Shelton et al., 2019). Moreover, only few radiometric ages are available for MVT deposits: e.g., Rb-Sr on sphalerite (Ostendorf et al., 2015; 2017); U-Pb/Th-Pb on carbonates (Brannon et al., 1996); and Re-Os on pyrite (Hnatyshin et al., 2015). This paucity of data on the absolute time differences between host-rock formation, dolomitization, and ore-mineral precipitation has generated controversy concerning shallow vs. deep burial depth and extensional vs. compressional tectonic settings for MVT formation (Leach et al., 2001; Kesler et al., 2004; Ostendorf et al., 2015).

This study presents the first radiometric ages for the Gorno district in Lombardy (N Italy), an example of the Alpine-type (APT) subclass of MVT deposits. APT deposits mostly occur as stratabound bodies within Anisian-Carnian platform carbonates across the Alps (Leach et al., 2003). Their genesis is still controversial since radiometric age data, only available for the Austrian deposit of Bleiberg, are highly uncertain: Sr and Pb isotopes on whole rock samples

gave errors of ± 30 and 48 my, respectively (Schroll et al., 2006); and Rb-Sr dating on sphalerite provided both Late Triassic and Early Jurassic ages (Henjes-Kunst et al., 2017, and references therein).

Based on the presence of finely-laminated ore textures, ore-bearing clasts in sedimentary breccias, and highly negative $\delta^{34}S$-values of the sulfide minerals, some authors suggest that several APT deposits formed shortly after, or even during host sediment deposition (e.g., Maucher and Schneider, 1967; Brigo et al., 1977; Cerny, 1989; Kucha et al., 2010). Others suggest a deep burial setting, based on high fluid-inclusion homogenization temperatures and comparison with classic MVT models (e.g., Jicha, 1951; Omenetto, 1966; Leach et al., 2003; Mondillo et al., 2019). A precise understanding of the timing and mode of ore formation is not only of scientific interest but also of economic relevance since it strongly affects current and future exploration.

Our U-Pb ages, obtained from hydrothermal carbonates closely associated with the ore minerals, combined with detailed petrographic and fluid inclusion data, provide a major advance in understanding the timing of APT Zn (-Pb) mineralization.

MATERIALS AND METHODS

Nineteen samples were collected for this study and investigated by transmitted light (TL) and cathodoluminescence (CL) microscopy. Fluid inclusion (FI) petrography and microthermometry were carried out on representative dolomite samples (doubly-polished sections 110 µm-thick). Carbonate U-Pb data were acquired by laser ablation inductively coupled plasma mass spectrometry (LA-ICP-MS) on polished thin sections (60 µm) following the methods of Roberts

et al. (2017) and Guillong et al. (2020). Details on the samples and analytical procedures are provided in the Supplementary Material.

GEOLOGICAL SETTING

The Gorno district lies in the Southalpine domain (Figs 1A and 1C), a south-verging retro-belt of the Alpine orogenic wedge, separated from the highly metamorphosed part of the Alps by the Periadriatic Line. The Southalpine domain consists of a thick sedimentary succession of Permian to Paleogene age, deformed during the Alpine orogeny (~80-38 Ma) under non-metamorphic conditions (Laubscher, 1985; Zanchi et al., 2012; Zanchetta et al., 2015). In the Gorno area, platform carbonate sedimentation took place from the late Anisian (Esino Limestone), briefly interrupted by emersion of the platform and development of subaerial karst and paleosols (Calcare Rosso) (Berra and Carminati, 2010; Jadoul et al., 2012) (Fig. 1B). In the early Carnian, the deposition of the 50-100 m-thick peritidal limestones of the Breno Formation (BF) was followed by the m- to tens of m-thick peritidal-lagoon facies of the Calcare Metallifero Bergamasco (CMB). A deepening of the basin then led to the deposition of the lagoonal marly limestones of the Gorno Formation (GF, >250 m-thick), which laterally pass into the stratigraphically equivalent deltaic volcaniclastic sediments of the Val Sabbia Sandstone. In the late Carnian, a return to shallow-water deposition was recorded by the sabkha dolostones and evaporites of the S. Giovanni Bianco Formation. The Gorno ore deposits are stratabound and confined to the lower Carnian stratigraphic interval (Fig. 1B). They mainly consist of sphalerite, minor galena, fluorite and barite. High-grade sulfide ore is hosted in the 5-10 m-thick basal unit of the GF, consisting of an organic-rich laminated marl and siltstone lithozone, historically known as “black shales”. Other major orebodies are hosted in the peritidal limestones of the BF

and CMB. Mineralization styles encompass replacements, dissolution cavity fillings, and breccia cements (Omenetto, 1966; Assereto et al., 1977; Mondillo et al., 2019). Current exploration efforts focus on the Zorzone and Pian Bracca deposits (Fig. 1B) and have identified a total resource of 7.79 Mt at 6.8% Zn, 1.8% Pb and 32 g/t Ag (Altamin, 2021).

PARAGENETIC SEQUENCE

A fabric-retentive, early diagenetic dolomite (Dol-1) replaces the micritic matrix of the supratidal laminated sediments of the BF and CMB. It is fine-grained, white in hand specimen, and exhibits bright-red CL. Lags of dolomitized intraclasts at the base of calcareous transgressive subtidal levels show that Dol-1 formed shortly after sedimentation (Fig. 2A). Fenestral pores in both unaltered limestones and Dol-1 dolostones are filled with a sparry calcite cement (Cal-1), commonly non-luminescent or dull-brown and locally zoned under CL (Fig. 3A-B).

A complex series of dolomitization, brecciation, dissolution, and cementation phenomena followed Dol-1 and Cal-1 and affected the studied rocks over the whole area (Fig. 4). Dolomitization gave rise to decametric, tan-colored bodies (replacive Dol-2), either roughly stratiform or less commonly discordant to the bedding (Fig. 1D). Replacive Dol-2 forms a mosaic of fine to coarse-grained euhedral dolomite crystals (30 to 600 μm) (Figs 3C-D). Dol-2 also occurs as coarsely crystalline saddle dolomite cements (up to mm-size) in pores, veins, burrow infills, and bivalve shell pseudomorphs (Figs 2E, G and 3C-D). Dol-2 is commonly dull red to almost non-luminescent under CL (Figs 3D and 3F). Primary FIs in Dol-2 cements yield homogenization temperatures between ~80 and 140 °C (mean value: 111 ± 13 °C; Table DR5; Supplementary Material). Dol-2 dolostone bodies are locally associated with crackle-to-mosaic breccias with cm- to dm-sized clasts mainly cemented by sphalerite and a calcite cement younger

than Cal-1 (Cal-2: see below) (Figs 2B-D). A major dissolution phase followed Dol-2 and is documented by irregularly shaped dm- to m-sized cavities with branches that are either roughly concordant or discordant to bedding (Figs 2F-G). Dissolution cavities show infills of laminated internal sediments consisting of dissolution residues such as host-rock clasts, mm- to cm-sized reworked fragments of Dol-2 cements in a finer carbonate matrix. Internal sediments are cemented by fluorite, Cal-2, or sulfides. A further saddle dolomite generation (Dol-3), mostly dull brown in CL, fills a stockwork of veinlets crossing Dol-2 dolomitized bodies. Locally, Dol-3 syntaxially overgrows Dol-2 cements in larger veins and fenestral pores, and reworked Dol-2 clasts in dissolution cavity infills (Figs 3C-F). Homogenization temperatures from primary FIs in Dol-3 cements range between ~80 and 140 °C (mean value: 107 ± 12 °C). Euhedral terminations of Dol-3 crystals are overgrown by sphalerite showing that sulfide precipitation directly followed Dol-3 (Figs 3C-F). Sphalerite commonly forms equant crystals up to mm-sized, occurring both as void filling cements and as replacement of the carbonate host (Figs 2B-D and 3C-H). A post-sulfide sparry calcite cement (Cal-2), up to cm-sized, fills the remaining voids in pores, veins and dissolution cavities (Figs 2B-D and 2F). Cal-2 shows an almost homogeneous bright-yellow CL and, depending on the site, overgrows either Cal-1, Dol-2, Dol-3 or sphalerite (Figs 3A and 3E-H). Locally, the Cal-1/Cal-2 boundary is irregular and cuts through CL zones in Cal-1, showing that Cal-2 precipitation occurred after etching of Cal-1 (Fig. 3B). Cal-2 also fills thin veins locally associated in swarms and merging with cavity-filling Cal-2 cements. This documents a fracturing event, taking place along with Cal-2 precipitation, which enhanced fluid circulation. More generally, the undolomitized host sediments (Fig. 3A-B), and early calcite cements only locally preserved in molds of large bivalve shells, show the same bright yellow CL, pointing to large-scale recrystallization coeval with Cal-2. Fluorite may occur together with Cal-2, showing

variable geometric relationships, suggesting coprecipitation of the two minerals. In conclusion, only two pore-filling calcite cement generations are recognizable over the whole study area. Therefore, all the yellow-luminescent calcite is referrable to Cal-2 and postdates sphalerite. Additional petrographic data are provided in the Supplementary Materials.

CARBONATE U-Pb GEOCHRONOLOGY

A total of nine measurement sites from five carbonate samples (out of the eight investigated) provided robust radiometric ages (Figs 4B-C; full age data in Tables DR3-4 and Fig. DR1 of the Supplementary Material). The earliest mineral in the paragenetic sequence (Dol-1) yielded an age of 245.8 ± 12.5 Ma (95% confidence interval). Pre-sulfide replacive and void-filling Dol-2 yielded ages of 229.9 ± 11.2 and 227.1 ± 17.9 Ma, respectively, while post-sulfide Cal-2 yielded ages of 232.2 ± 5.2, 229.0 ± 10.8, 228.4 ± 5.3 and 226.9 ± 5.3 Ma. All these ages fall within a relatively narrow range, and overlap or shortly postdate the early Carnian depositional age of the host rocks (~237-232 Ma) (Fig. 4B). A younger age of replacive Dol-2 (96.5 ± 16.4 Ma) can be explained by recrystallization of the fine-grained dolomite due to high burial temperatures during the Cretaceous (Carminati et al., 2010). Another younger age produced from a Dol-2 cement (139.9 ± 33.8) is difficult to interpret, but probably reflects a resetting process.

DISCUSSION AND CONCLUSIONS

The U-Pb radiometric ages presented in this paper provide the first robust constraints on the age of ore formation in the Gorno area. The younger age limit is given by the precipitation age of post-sulfide Cal-2 (227.0-232.2 Ma, i.e., the overlap between the four Cal-2 ages). Conversely, the older age limit is defined by the precipitation of pre-sulfide Dol-2 and by host-rock

deposition (early Carnian; ~232-237 Ma). Consequently, all processes ranging from Dol-2 to Cal-2 precipitation, which include dissolution, brecciation, and sulfide precipitation, must fall in a time window of some million years after the deposition of the host rocks. Thus, the burial depth at the time of ore formation was relatively shallow (tens to a few hundreds of meters), based on the known thicknesses of the overlying sediments (GF/Val Sabbia and San Giovanni Bianco formations and the lowermost part of Dolomia Principale: Jadoul et al., 2012). Homogenization temperatures obtained from primary FIs in pre-ore hydrothermal dolomites (Dol-2; Dol-3) range between ~80° and 140°C. These results and the observed carbonate paragenesis are closely comparable to those reported by Hou et al. (2016) for the same area. However, these authors could not rely on radiometric ages, and thus interpreted these formation temperatures as a result of deep burial. In the light of our new radiometric data and inferred shallow burial depths, the homogenization temperatures are too high to be caused by the burial load alone, even if the maximum burial depth and a high geothermal gradient of 40°C/km (for continental areas of extension: Jaupart and Mareschal, 2007) are assumed. Thus, they clearly indicate the presence of thermal disequilibrium between the fluids and host rocks. High crustal heat flux was likely at that time: in fact, regional magmatism linked to extensional and strike-slip tectonics (Doglioni, 1987; Berra and Carminati, 2010) is well documented in the Southalpine domain during the Anisian-Carnian, related to an early phase of Pangea breakup (De Min et al., 2020, and references therein). In the Gorno district, pyroclastic layers in the lower Carnian BF and CMB, and volcaniclastic deposits in the overlying Val Sabbia Sandstone provide the main evidence for magmatism (Jadoul et al., 2012). While a direct genetic link between sulfide mineralization and magmatism cannot be inferred from the available data, it is likely that magmatic activity contributed to the high heat fluxes necessary to drive a hydrothermal system

in the Gorno district. Concurrent thermal perturbation and extensional faulting triggered the upward flow of metal-rich fluids from depth, e.g., from crystalline basement rocks, resulting in sulfide deposition within the carbonate sediments.

The classic MVT model, envisaging circulation of basinal brines in foreland settings, was originally defined for the deposits in the drainage basin of the Mississippi River. This model relates high precipitation temperatures to deep burial, and has often been applied to other carbonate-hosted Pb-Zn deposits worldwide. However, its general applicability has been challenged since new geochronologic data showed that MVT deposits can also form at shallow depths in extensional settings, and possibly related to magmatism (e.g., Twelve Mile Bore and Bloodwood-Kapok in Western Australia, Brannon et al., 1996; Maestrat basin in Spain, Grandia et al., 2000; Irish Midlands, Hnatyshin et al., 2015; Jabali in Yemen, Ostendorf et al., 2015; Tres Marias in Mexico, Ostendorf et al., 2017).

The Gorno case represents a further example of an MVT deposit formed at shallow burial depth and in an extensional setting, and thus confirms the need for solid geochronological data to construct reliable metallogenic models. In the absence of age data, any correlation between precipitation temperatures and burial depths is highly questionable, and inferences about geodynamic settings are purely speculative. The term MVT encompasses a broad range of sulfide deposits formed under different conditions and should thus be used with a purely descriptive meaning, avoiding genetic implications.

ACKNOWLEDGMENTS

We thank Altamin, Ltd. (Perth, Australia), for the fruitful collaboration. T. Blaise, D. Chew, an anonymous reviewer, and editor W. Clyde provided constructive suggestions. This paper is dedicated to the memory of P. Rossetti, who first conceptualized the idea of this research.

REFERENCES CITED

Assereto, R., Jadoul, F., and Omenetto, P., 1977, Stratigrafia e metallogenesi del settore occidentale del distretto a Pb, Zn, fluorite e barite di Gorno (Alpi Bergamasche): Rivista Italiana di Paleontologia e Stratigrafia, v. 83, p. 395–532.

Altamin Ltd., 2021, ASX announcement - Major mineral resource upgrade at Gorno: https://clients3.weblink.com.au/pdf/AZI/02395048.pdf (accessed August 2021).

Berra, F., and Carminati, E., 2010, Subsidence history from a backstripping analysis of the Permo-Mesozoic succession of the Central Southern Alps (Northern Italy): Basin Research, v. 22, p. 952–975, doi:10.1111/j.1365-2117.2009.00453.x.

Brannon, J.C., Cole, S.C., Podosek, F.A., Ragan, V.M., Coveney, R.M., Wallace, M.W., and Bradley, A.J., 1996, Th-Pb and U-Pb Dating of Ore-Stage Calcite and Paleozoic Fluid Flow: Science, v. 271, p. 491–493, doi:10.1126/science.271.5248.491.

Brigo, L., Kostelka, L., Omenetto, P., Schneider, H.-J., Schroll, E., Schulz, O., and Štrucl, I., 1977, Comparative reflections on four Alpine Pb-Zn deposits, in Klemm, D.D., and Schneider, H.-J., eds., Time and strata-bound ore deposits: Berlin, Heidelberg, Springer, p. 273–293, doi:10.1007/978-3-642-66806-7_18.

Carminati, E., Cavazza, D., Scrocca, D., Fantoni, R., Scotti, P., and Doglioni, C., 2010, Thermal and tectonic evolution of the Southern Alps (northern Italy) rifting: Coupled organic matter maturity analysis and thermokinematic modeling: AAPG Bulletin, v. 94, p. 369–

397, doi:10.1306/08240909069.

Cerny, I., 1989, Die karbonatgebundenen Blei-Zink-Lagerstätten des alpinen und ausser-alpinen Mesozoikums: Die Bedeutung ihrer Geologie, Stratigraphie und Faziesgebundenheit für Prospektion und Bewertung; Les gisements Pb-Zn liés aux carbonates du Mésozoïque alpin et extr: Archiv für Lagerstättenforschung der Geologischen Bundesanstalt, v. 11, p. 5–125.

De Min, A., Velicogna, M., Ziberna, L., Chiaradia, M., Alberti, A., and Marzoli, A., 2020, Triassic magmatism in the European Southern Alps as an early phase of Pangea break-up: Geological Magazine, v. 157, p. 1800–1822, doi:10.1017/S0016756820000084.

Doglioni, C., 1987, Tectonics of the Dolomites (Southern Alps, Northern Italy): Journal of Structural Geology, v. 9, p. 181–193, doi:10.1016/0191-8141(87)90024-1.

Grandia, F., Asmerom, Y., Getty, S., Cardellach, E., and Canals, À., 2000, U–Pb dating of MVT ore-stage calcite: implications for fluid flow in a Mesozoic extensional basin from Iberian Peninsula: Journal of Geochemical Exploration, v. 69–70, p. 377–380, doi:10.1016/S0375-6742(00)00030-3.

Guillong, M., Wotzlaw, J.F., Looser, N., and Laurent, O., 2020, Evaluating the reliability of U-Pb laser ablation inductively coupled plasma mass spectrometry (LA-ICP-MS) carbonate geochronology: Matrix issues and a potential calcite validation reference material: Geochronology, v. 2, p. 155–167, doi:10.5194/gchron-2-155-2020.

Henjes-Kunst, E., Raith, J.G., and Boyce, A.J., 2017, Micro-scale sulfur isotope and chemical variations in sphalerite from the Bleiberg Pb-Zn deposit, Eastern Alps, Austria: Ore Geology Reviews, v. 90, p. 52–62, doi:10.1016/j.oregeorev.2017.10.020.

Hnatyshin, D., Creaser, R.A., Wilkinson, J.J., and Gleeson, S.A., 2015, Re-Os dating of pyrite

confirms an early diagenetic onset and extended duration of mineralization in the Irish Zn-Pb ore field: Geology, v. 43, p. 143–146, doi:10.1130/G36296.1.

Jadoul, F., Berra, F., Bini, A., Ferliga, C., Mazzoccola, D., Papani, L., Piccin, A., Rossi, R., Rossi, S., and Trombetta, G.L., 2012, Note illustrative della Carta Geologica d'Italia alla scala 1: 50.000, Foglio 077 "Clusone": Treviso, Servizio Geologico d'Italia, ISPRA (Istituto Superiore per la Protezione e la Ricerca Ambientale), Regione Lombardia, 120 p.

Jaupart, C., and Mareschal, J.-C., 2007, Heat flow and thermal structure of the lithosphere, *in* Schubert, G., and Watts, A.B., eds., Treatise on Geophysics, v. 6: London, Elsevier, p. 217–251, doi:10.1016/B978-044452748-6/00104-8.

Jicha, H.L., 1951, Alpine lead-zinc ores of Europe: Economic Geology, v. 46, p. 707–730, doi:10.2113/gsecongeo.46.7.707.

Kesler, S.E., Chesley, J.T., Christensen, J.N., Hagni, R.D., Heijlen, W., Kyle, J.R., Muchez, P., Misra, K.C., and Van der Voo, R., 2004, Discussion of "Tectonic controls of Mississippi Valley-type lead-zinc mineralization in orogenic forelands" by D.C. Bradley and D.L. Leach: Mineralium Deposita, v. 39, p. 512–514, doi:10.1007/s00126-004-0422-3.

Kucha, H., Schroll, E., Raith, J.G., and Halas, S., 2010, Microbial sphalerite formation in carbonate-hosted Zn-Pb ores, Bleiberg, Austria: Micro to nanotextural and sulfur isotope evidence: Economic Geology, v. 105, p. 1005–1023, doi:10.2113/gsecongeo.105.5.1005.

Laubsher, H.P., 1985, Large-scale, thin-skinned thrusting in the southern Alps: Kinematic models: GSA Bulletin, v. 96, p. 710–718, doi:10.1130/0016-7606(1985)96<710:LTTITS>2.0.CO;2.

Leach, D.L., Bradley, D., Lewchuk, M.T., Symons, D.T.A., de Marsily, G., and Brannon, J.,

2001, Mississippi Valley-type lead-zinc deposits through geological time: Implications from recent age-dating research: Mineralium Deposita, v. 36, p. 711–740, doi:10.1007/s001260100208.

Leach, D.L., Bechstädt, T., Boni, M., and Zeeh, S., 2003, Triassic-hosted Mississippi Valley-type zinc-lead ores of Poland, Austria, Slovenia, and Italy, *in* Kelly, J.G., Andrew, C.J. Ashton, J.H., Boland, M.B., Earls, G., Fusciardi, L., and Stanley, G., eds., Europe's major base metal deposits: Dublin, Ireland, Irish Association of Economic Geologists, p. 169–213.

Leach, D.L., Sangster, D.F., Kelley, K.D., Large, R.R., Garven, G., Allen, C.R., Gutzmer, J., and Walters, S., 2005, Sediment-hosted lead-zinc deposits: A global perspective: Economic Geology, v. 100, p. 561–607.

Maucher, A., and Schneider, H.-J., 1967, The Alpine lead-zinc ores, *in* Brown, J.S., ed., Genesis of lead-zinc-barite-fluorite deposits in carbonate rocks (the so-called Mississippi Valley type deposits): Lancaster, Pennsylvania, Economic Geology Monograph 3, p. 71–89.

Mondillo, N., Lupone, F., Boni, M., Joachimski, M., Balassone, G., De Angelis, M., Zanin, S., and Granitzio, F., 2019, From Alpine-type sulfides to nonsulfides in the Gorno Zn project (Bergamo, Italy): Mineralium Deposita, v. 55, p. 953–970, doi:10.1007/s00126-019-00912-5.

Omenetto, P., 1966, Il giacimento piombo-zincifero di Oltre il Colle (Alpi bergamasche): Memorie degli Istituti di Geologia e Mineralogia dell'Università di Padova, v. 25, p. 3–49.

Ostendorf, J., Henjes-Kunst, F., Mondillo, N., Boni, M., Schneider, J., and Gutzmer, J., 2015, Formation of Mississippi Valley–type deposits linked to hydrocarbon generation in

extensional tectonic settings: Evidence from the Jabali Zn-Pb-(Ag) deposit (Yemen): Geology, v. 43, p. 1055–1058, doi:10.1130/G37112.1.

Ostendorf, J., Henjes-Kunst, F., Schneider, J., Melcher, F., and Gutzmer, J., 2017, Genesis of the carbonate-hosted Tres Marias Zn-Pb-(Ge) deposit, Mexico: Constraints from Rb-Sr sphalerite geochronology and Pb isotopes: Economic Geology, v. 112, p. 1075–1087, doi:10.5382/econgeo.2017.4502.

Roberts, N.M.W., Rasbury, E.T., Parrish, R.R., Smith, C.J., Horstwood, M.S.A., and Condon, D.J., 2017, A calcite reference material for LA-ICP-MS U-Pb geochronology: Geochemistry, Geophysics, Geosystems, v. 18, p. 2807–2814, doi:10.1002/2016GC006784.

Schroll, E., Köppel, V., and Cerny, I., 2006, Pb and Sr isotope and geochemical data from the Pb–Zn deposit Bleiberg (Austria): Constraints on the age of mineralization: Mineralogy and Petrology, v. 86, p. 129–156, doi:10.1007/s00710-005-0107-3.

Shelton, K.L., Hendry, J.P., Gregg, J.M., Truesdale, J.P., and Somerville, I.D., 2019, Fluid circulation and fault- and fracture-related diagenesis in Mississippian syn-rift carbonate rocks on the northeast margin of the metalliferous Dublin Basin, Ireland: Journal of Sedimentary Research, v. 89, p. 508–536, doi:10.2110/jsr.2019.31.

Zanchetta, S., Malusà, M.G., and Zanchi, A., 2015, Precollisional development and Cenozoic evolution of the Southalpine retrobelt (European Alps): Lithosphere, v. 7, p. 662–681, doi:10.1130/L466.1.

Zanchi, A., D'Adda, P., Zanchetta, S., and Berra, F., 2012, Syn-thrust deformation across a transverse zone: The Grem–Vedra fault system (central Southern Alps, N Italy): Swiss Journal of Geosciences, v. 105, p. 19–38, doi:10.1007/s00015-011-0089-6.

FIGURE CAPTIONS

Figure 1. (A) Schematic geological map of the Alps. (B) Stratigraphic log of the upper Anisian-Carnian succession, showing the main mineralized horizons. (C) Geological map of the Gorno district showing the main ore deposits. 1: upper Carnian-Norian carbonates. 2: San Giovanni Bianco Fm.; Val Sabbia Sandstone; GF. 3: CMB; BF.; Calcare Rosso. 4: upper Anisian-Ladinian carbonates. 5: faults. 6: thrusts. 7: historic mines. 8: mines in exploration phase. Adapted from Jadoul et al. (2012). (D) Field features of stratabound Dol-2 bodies in the CMB (below the dashed line), hosting major sulfide mineralization (45°55'15.1"N - 9°48'07.9"E).

Figure 2. (A) Lags of Dol-1 intraclasts at the base of transgressive subtidal levels in the CMB. (B) Stratiform crackle breccia with Dol-2 clasts cemented by sphalerite (Sp) and Cal-2. (C) Mesoscopic features and (D) thin section scan of sample OC89, showing typical Dol-2, sphalerite (Sp), and Cal-2 relationships in mineralized breccias. (E) Bivalve shell pseudomorphs with Dol-2 infills in the CMB. (F) Dissolution cavity in the BF (delimited by dashed line), infilled by laminated sediments (lsed) deposited on euhedral terminations of Cal-2 crystals. (G) Internal sediments in a dissolution cavity in the BF (base delimited by dashed line). A lag of Dol-2 clasts passes upwards into finer-grained laminated sediments (lsed).

Figure 3. Petrographic features: (A) TL and CL images (upper and lower half, respectively) of a shrinkage pore infilled by Cal-1 and Cal-2. (B) CL image of Cal-1 fenestral pore infills (delimited by the dotted line) suffering dissolution and reprecipitation. (C) TL and (D) CL images of a shrinkage pore (delimited by a white line) infilled by Dol-2, Dol-3a and sphalerite (Sp) cements. (E) TL and (F) CL images of reworked Dol-2 cements (delimited by a white line) in a dissolution cavity, overgrown by Dol-3a, sphalerite (Sp) and sparry Cal-2. (G) TL and (H)

CL images of Cal-2 filling irregularities and fractures in sphalerite (Sp). rxCal2 = recrystallized limestone; rDol-2 = replacive Dol-2.

Figure 4. (A) Simplified paragenetic sequence showing relative timing of the principal mineral phases. Dashed lines indicate uncertain ranges. (B) Selected U-Pb ages of carbonate minerals with associated error bars. Also indicated are the age and the estimated burial depth of the host rock in relation to age. (C) Selected Tera-Wasserburg concordia diagrams of ore-related carbonates. Full U-Pb age data in the Supplementary Material.

[1]GSA Data Repository item 201Xxxx, including extended Materials and Methods, additional petrographic data for U-Pb geochronology, additional Tera-Wasserburg concordia diagrams, plus additional figures and tables, is available online at www.geosociety.org/pubs/ft20XX.htm, or on request from editing@geosociety.org.

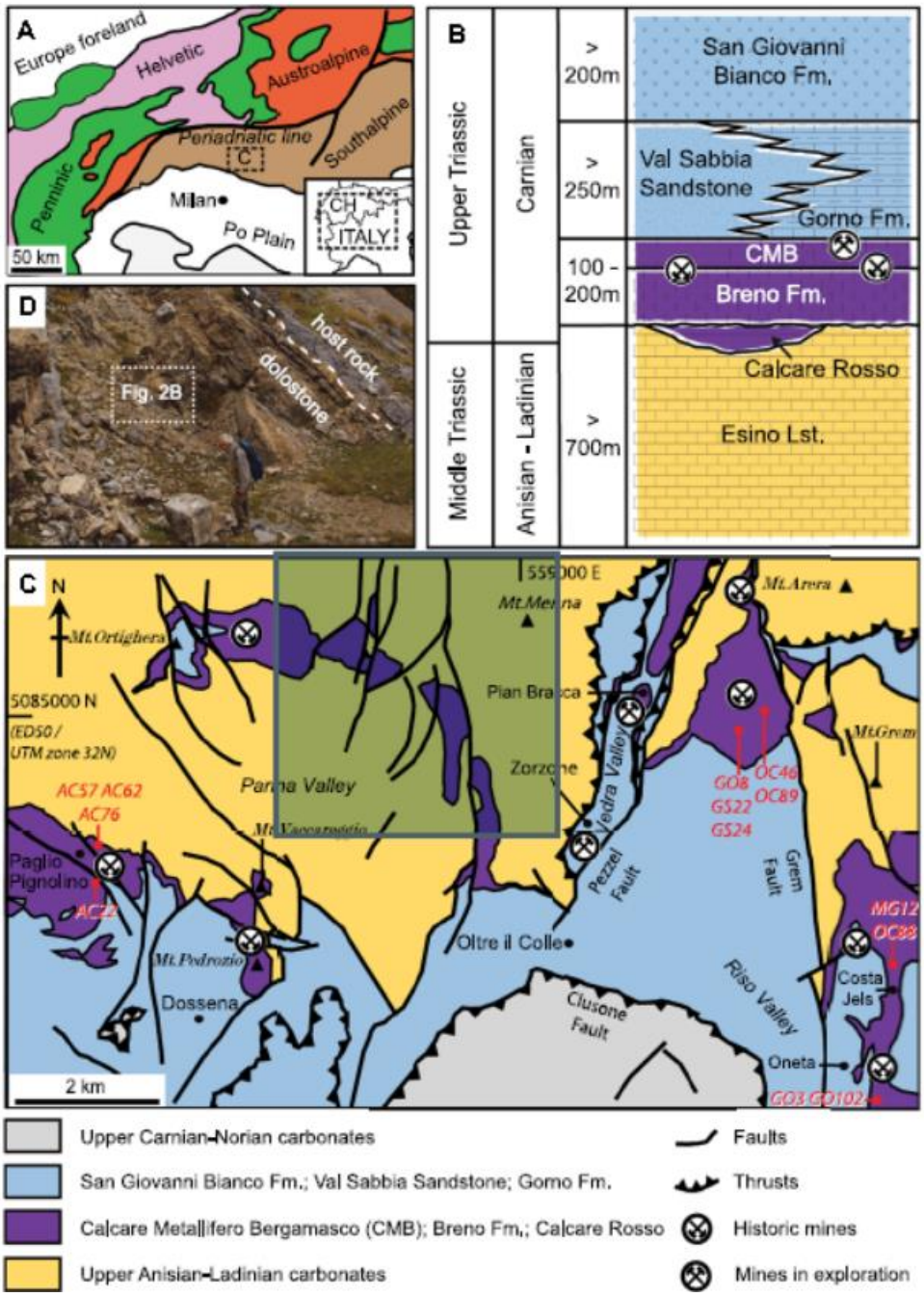
A
Europe foreland
Helvetic
Austroalpine
Penninic
Periadriatic line
Southalpine
Milan
Po Plain
CH
ITALY
50 km
B
Upper Triassic
Carnian
Middle Triassic
Anisian - Ladinian
> 200m
San Giovanni Bianco Fm.
> 250m
Val Sabbia Sandstone
Gorno Fm.
CMB
100 - 200m
Breno Fm.
Calcare Rosso
> 700m
Esino Lst.
D
Fig. 2B
host rock
dolostone
C
N
Mt.Ortighera
5085000 N
(ED50 / UTM zone 32N)
559000 E
Mt.Arera
Mt.Menna
Pian Bracca
Mt.Grem
Parina Valley
Zorzone
Vedra Valley
AC57 AC62
AC76
GO8 OC46
GS22 OC89
GS24
Paglio Pignolino
AC77
Pezzel Fault
Grem Fault
MG12
OC33
Mt.Vaccaroggio
Mt.Pedrozio
Oltre il Colle
Costa Jels
Dossena
Clusone Fault
Riso Valley
Oneta
GO3 GO102
2 km
Upper Carnian-Norian carbonates
San Giovanni Bianco Fm.; Val Sabbia Sandstone; Gorno Fm.
Calcare Metallifero Bergamasco (CMB); Breno Fm.; Calcare Rosso
Upper Anisian-Ladinian carbonates
Faults
Thrusts
Historic mines
Mines in exploration

Fig. 1

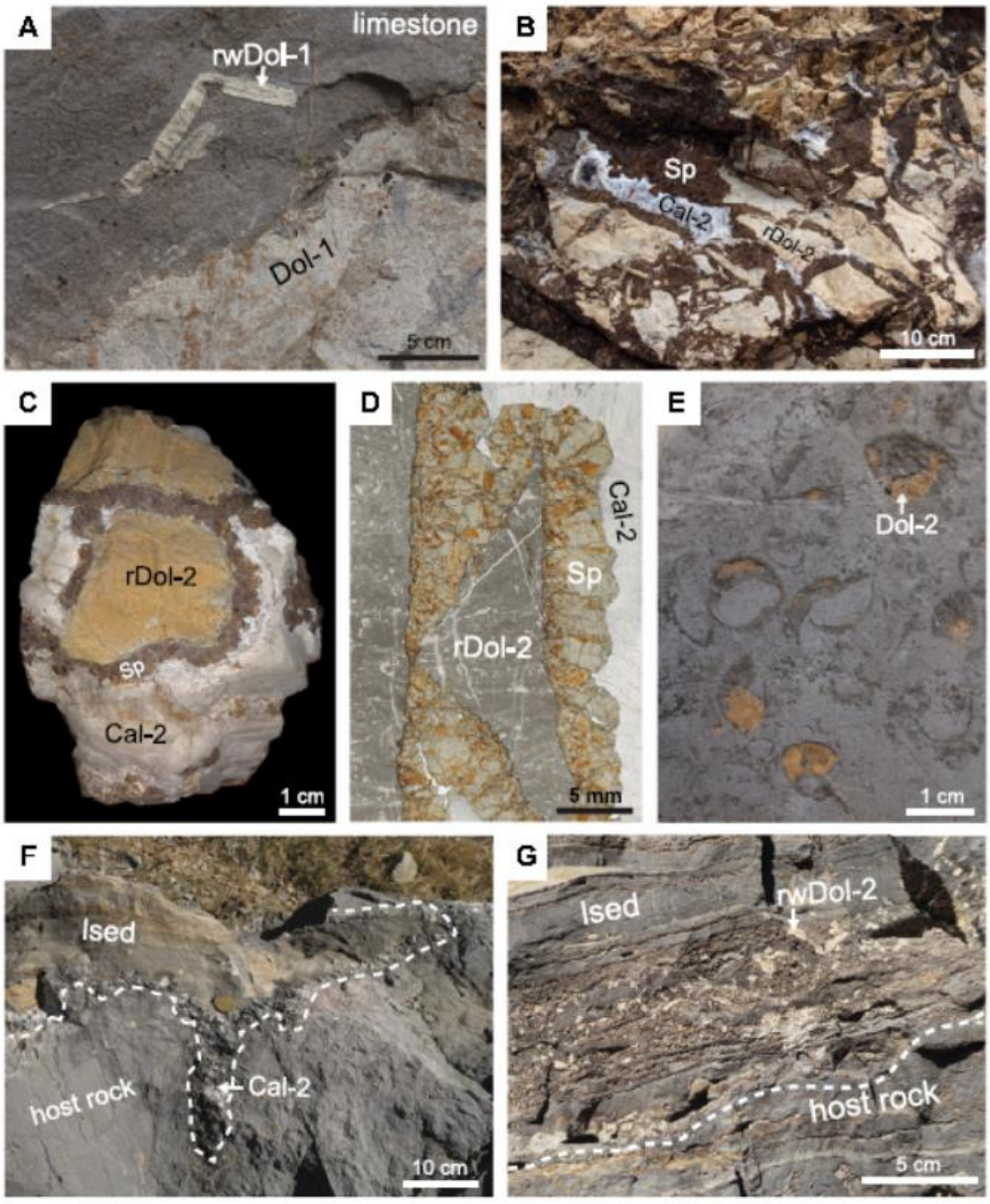
A
limestone
rwDol-1
Dol-1
5 cm
B
Sp
Cal-2
rDol-2
10 cm
C
rDol-2
Sp
Cal-2
1 cm
D
Cal-2
Sp
rDol-2
5 mm
E
Dol-2
1 cm
F
lsed
host rock
Cal-2
10 cm
G
lsed
rwDol-2
host rock
5 cm

Fig. 2

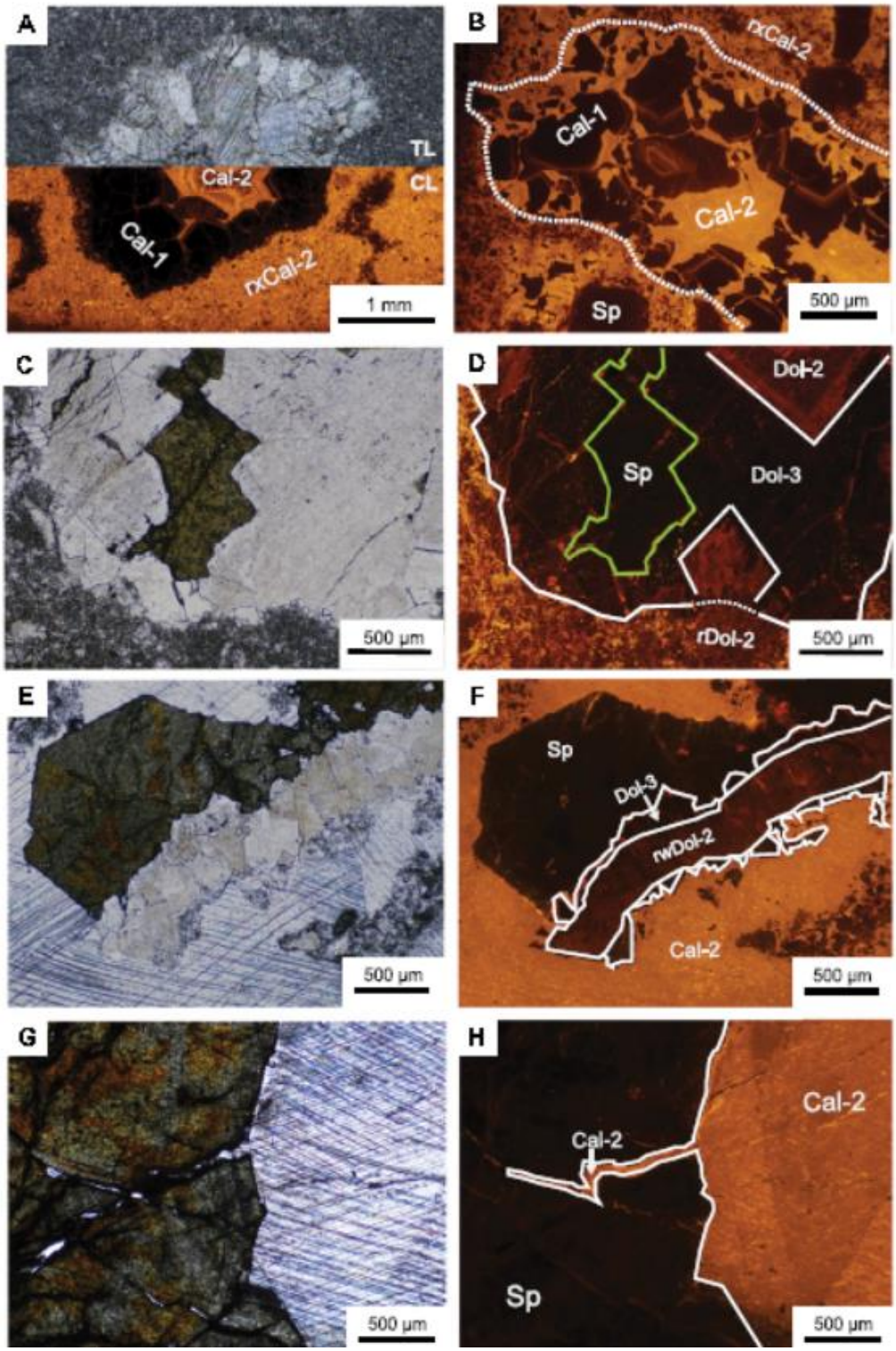
A
TL
Cal-2
CL
Cal-1
rxCal-2
1 mm
B
rxCal-2
Cal-1
Cal-2
Sp
500 µm
C
500 µm
D
Dol-2
Sp
Dol-3
rDol-2
500 µm
E
500 µm
F
Sp
Dol-3
rwDol-2
Cal-2
500 µm
G
500 µm
H
Cal-2
Cal-2
Sp
500 µm

Fig. 3

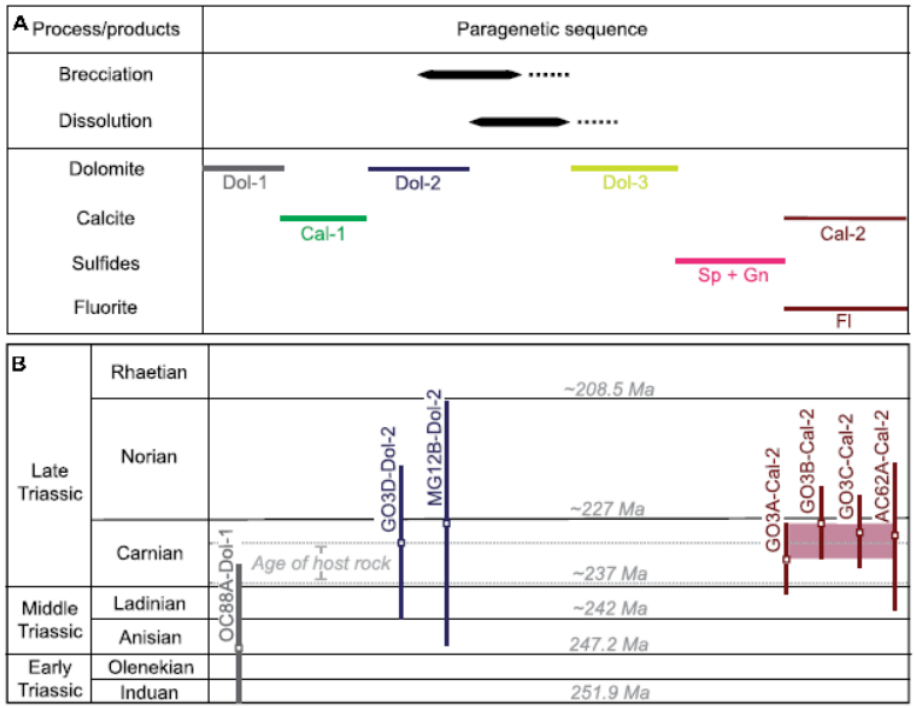
A
Process/products
Paragenetic sequence
Brecciation
Dissolution
Dolomite
Calcite
Sulfides
Fluorite
Dol-1
Dol-2
Dol-3
Cal-1
Cal-2
Sp + Gn
Fl
B
Rhaetian
Late Triassic
Norian
Carnian
Middle Triassic
Ladinian
Anisian
Early Triassic
Olenekian
Induan
~208.5 Ma
~227 Ma
~237 Ma
~242 Ma
247.2 Ma
251.9 Ma
GO3D-Dol-2
MG12B-Dol-2
GO3A-Cal-2
GO3B-Cal-2
GO3C-Cal-2
AC62A-Cal-2
OC88A-Dol-1
Age of host rock

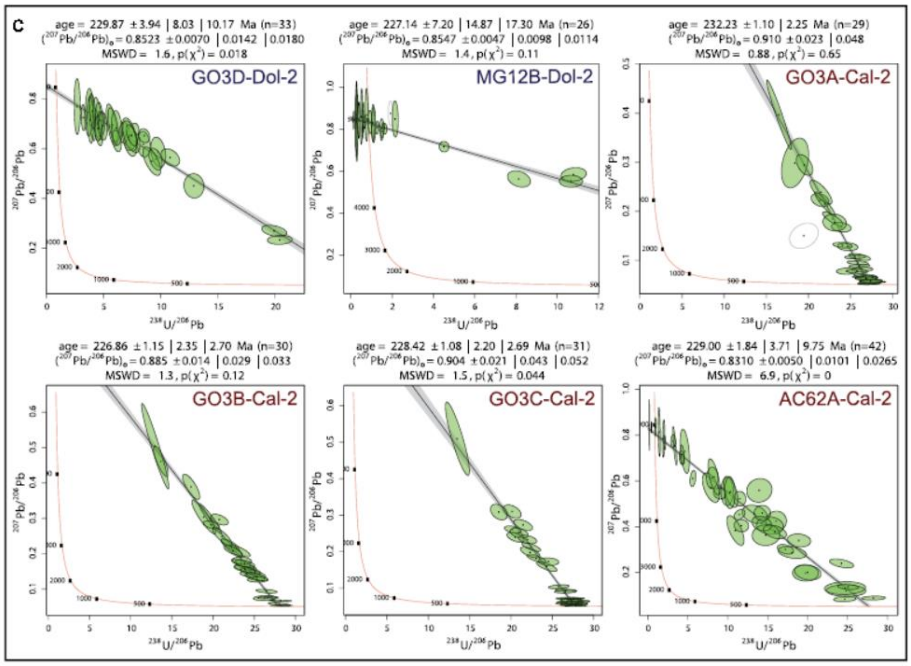
C
GO3D-Dol-2
MG12B-Dol-2
GO3A-Cal-2
GO3B-Cal-2
GO3C-Cal-2
AC62A-Cal-2

Fig. 4